Monthly Notices
of the
ROYAL ASTRONOMICAL SOCIETY

MNRAS **471,** 4314–4322 (2017)
Advance Access publication 2017 July 20

doi:10.1093/mnras/stx1825

Distribution functions for resonantly trapped orbits in the Galactic disc

Giacomo Monari,[1]★ Benoit Famaey,[2] Jean-Baptiste Fouvry[3]† and James Binney[4]

[1]*The Oskar Klein Centre for Cosmoparticle Physics, Department of Physics, Stockholm University, AlbaNova, SE-10691 Stockholm, Sweden*
[2]*Observatoire astronomique de Strasbourg, Université de Strasbourg, CNRS UMR 7550, 11 rue de l'Université, F-67000 Strasbourg, France*
[3]*Institute for Advanced Study, Einstein Drive, Princeton, NJ 08540, USA*
[4]*Rudolf Peierls Centre for Theoretical Physics, Keble Road, Oxford OX1 3NP, UK*

Accepted 2017 July 17. Received 2017 July 17; in original form 2017 June 12

ABSTRACT

The present-day response of a Galactic disc stellar population to a non-axisymmetric perturbation of the potential has previously been computed through perturbation theory within the phase-space coordinates of the unperturbed axisymmetric system. Such an *Eulerian* linearized treatment, however, leads to singularities at resonances, which prevent quantitative comparisons with data. Here, we manage to capture the behaviour of the distribution function (DF) at a resonance in a *Lagrangian* approach, by averaging the Hamiltonian over fast angle variables and re-expressing the DF in terms of a new set of canonical actions and angles variables valid in the resonant region. We then follow the prescription of Binney, assigning to the resonant DF the time average along the orbits of the axisymmetric DF expressed in the new set of actions and angles. This boils down to phase-mixing the DF in terms of the new angles, such that the DF for trapped orbits depends only on the new set of actions. This opens the way to quantitatively fitting the effects of the bar and spirals to *Gaia* data in terms of DFs in action space.

Key words: Galaxy: disc – Galaxy: kinematics and dynamics – Galaxy: structure.

1 INTRODUCTION

The optimal exploitation of the next data releases of the *Gaia* mission (Gaia Collaboration et al. 2016) will necessarily involve the construction of a fully dynamical model of the Milky Way. Rather than trying to construct a quixotic full *ab initio* hydrodynamical model of the Galaxy, which would never be able to reproduce all the details of the *Gaia* data, a promising approach is to rather construct a multicomponent phase-space distribution function (DF) representing each stellar population as well as dark matter, and to compute the potential that these populations jointly generate (e.g. Binney & Piffl 2015). To do so, one can make use of the Jeans theorem, constraining the DF of an equilibrium configuration to depend only on three integrals of motion. Choosing three integrals of motion that have canonically conjugate variables allows us to express the Hamiltonian H_0 in its simplest form, i.e. depending only on these three integrals. Such integrals are called the 'action variables' $\boldsymbol{J}$, and are new generalized momenta having the dimension of velocity times distance, while their dimensionless canonically conjugate variables are called the 'angle variables' $\boldsymbol{\theta}$, because they are usually normalized such that the phase-space position is 2π-periodic in them (e.g. Binney & Tremaine 2008). In the absence of perturbations, these angles evolve linearly with time, $\boldsymbol{\theta}(t) = \boldsymbol{\theta}_0 + \boldsymbol{\Omega} t$, where $\boldsymbol{\Omega}(\boldsymbol{J}) \equiv \partial H_0/\partial \boldsymbol{J}$ is the vector of fundamental orbital frequencies. In an equilibrium configuration, the angle coordinates of stars are phase-mixed on orbital tori that are defined by the actions $\boldsymbol{J}$ alone, and the phase-space density of stars $f_0(\boldsymbol{J})\mathrm{d}^3\boldsymbol{J}$ corresponds to the number of stars $\mathrm{d}N$ in a given infinitesimal action range divided by $(2\pi)^3$. In an axisymmetric configuration, the action variables can simply be chosen to be the radial, azimuthal and vertical actions, respectively. By constructing DFs depending on these action variables, the current best axisymmetric models of the Milky Way have been constructed (Cole & Binney 2017).

The Milky Way is, however, not axisymmetric: It harbours both a bar (de Vaucouleurs 1964; Binney et al. 1991; Binney, Gerhard & Spergel 1997; Wegg, Gerhard & Portail 2015; Monari et al. 2017a,b) and spiral arms, the exact number, dynamics and nature of which are still under debate (Sellwood & Carlberg 2014; Grand et al. 2015). Whilst Trick et al. (2017) showed that spiral arms might not affect the axisymmetric fit, the combined effects of spiral arms and the central bar of the Milky Way are clearly important observationally (e.g. McMillan 2013; Bovy et al. 2015). Hence, non-axisymmetric DFs are needed to pin down the present structure of the non-axisymmetric components of the potential, which have enormous importance as drivers of the secular evolution of the disc

★ E-mail: giacomo.monari@fysik.su.se
† Hubble Fellow.

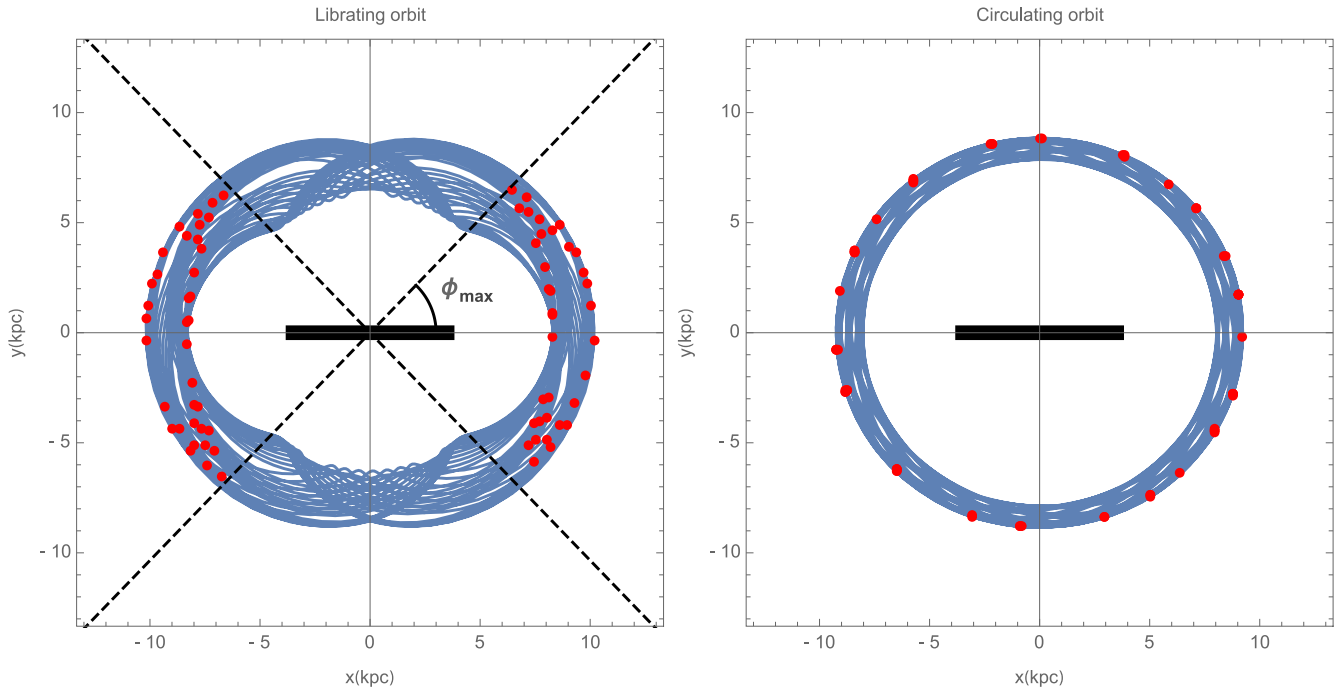

Figure 1. Two orbits in the Galactic potential described in this work, shown in the reference frame corotating with the bar. Here, the pattern speed is chosen to be $\Omega_b = 1.8\Omega_0$. The red points correspond to the position of the relative apocentres. The thick horizontal line represents the long axis of the bar. The bar rotates counterclockwise. Left-hand panel: an orbit trapped to the outer Lindblad resonance, where the angle ϕ_{max} (dashed lines) represents the maximum extension of the apocentres excursions. Right-hand panel: a circulating orbit.

(Fouvry, Binney & Pichon 2015; Fouvry, Pichon & Prunet 2015; Aumer, Binney & Schönrich 2016; Aumer & Binney 2017).

A recent step (Monari, Famaey & Siebert 2016) has been to derive from perturbation theory explicit DFs for present-day snapshots of the disc as a function of the actions and angles of the unperturbed axisymmetric system. This work, which is an *Eulerian* approach to the problem posed by non-axisymmetry, has allowed us to probe the effect of stationary spiral arms in three spatial dimensions, away from the main resonances. In particular, the moments of the perturbed DF describe 'breathing' modes of the Galactic disc in perfect accordance with simulations (Monari et al. 2016). Such a breathing mode might actually have been detected in the extended solar neighbourhood (Williams et al. 2013), but with a larger amplitude, perhaps because the spiral arms are transient. Although such an *Eulerian* treatment has also been used to gain *qualitative* insights into the effects of non-axisymmetries near resonances (Monari et al. 2017a), no quantitative assessments can be made with such an approach because the linear treatment diverges at resonances (the problem of small divisors; Binney & Tremaine 2008).

In the present contribution, we solve this problem by developing the *Lagrangian* approach to the impact of non-axisymmetries at resonances. The basic idea is to model the deformation of the orbital tori outside of the trapping region, and to construct new tori, complete with a new system of angle–action variables, within the trapping region (Kaasalainen 1994). Finally, following Binney (2016), we populate the new tori by phase-averaging the unperturbed DF over the new tori.

In Section 2, we present some examples of trapped and untrapped orbits. In Section 3, we summarize the standard approach to a resonance, namely to make a canonical transformation to fast and slow angles and actions, and to replace the real Hamiltonian with its average over the fast angles (Arnold 1978). Under this averaged Hamiltonian, the slow variables have the dynamics of a pendulum. In Section 4, we introduce the pendulum's angles and actions. In Section 5, we discuss how to build the DF using the newly introduced pendulum angles and actions, both inside and outside the zone of trapping at resonances. In Section 6, we present the form of the DFs in velocity space, in cases of astrophysical interest related to the Galactic bar. We conclude in Section 7.

2 THE BAR AND TRAPPED ORBITS

Let us consider orbits in the Galactic plane, and let (R, ϕ) be the Galactocentric radius and azimuth. The logarithmic potential, corresponding to a flat circular velocity curve $v_c(R) = v_0$, is a rough but simple representation of the potential of the Galaxy. In a formula,

$$\Phi(R) = v_0^2 \ln(R/R_0), \tag{1}$$

with R_0 the distance of the Sun from the Galactic centre. Motion in this planar axisymmetric potential admits actions J_ϕ, which is simply the angular momentum about the Galactic Centre, and J_R, which quantifies the extent of radial oscillations.

Let the axisymmetric potential be perturbed by a non-axisymmetric component

$$\Phi_1(R, \phi, t) = \mathrm{Re}\left\{\Phi_a(R) \mathrm{e}^{\mathrm{i}m(\phi - \Omega_b t)}\right\}, \tag{2}$$

where Ω_b is the pattern speed. We will specialize to the bar adopted by Dehnen (2000) and Monari et al. (2017a), so we set $m = 2$ and adopt

$$\Phi_a(R) = -\alpha_b \frac{R_0^5 \Omega_0^2}{3R_b^3} \times \begin{cases} (R/R_b)^{-3} & R \geq R_b, \\ 2 - (R/R_b)^3 & R < R_b, \end{cases} \tag{3}$$

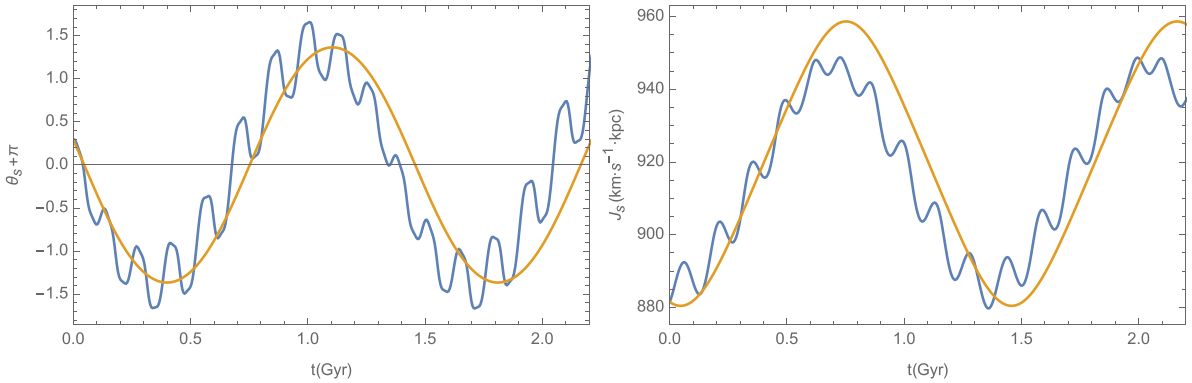

Figure 2. The slow variables $\theta_s + \pi$ (left-hand panel) and J_s (right-hand panel) for the librating orbit of Fig. 1. The blue lines correspond to the numerically integrated orbit and the orange lines to the pendulum approximation.

where $\Omega_0 \equiv \Omega(R_0)$ is the circular frequency at the solar radius, R_b is the length of the bar and α_b represents the maximum ratio between the radial force contributed by the bar and the axisymmetric background at the Sun (see also Monari, Famaey & Siebert 2015; Monari et al. 2016). We further set $R_0 = 8.2$ kpc, $v_0 = 243$ km s^{-1}, $R_b = 3.5$ kpc and $\alpha = 0.01$.

Fig. 1 shows for $\Omega_b = 1.8\Omega_0$ two orbits in the reference frame corotating with the bar. The red points in this plot correspond to the relative apocentres of the orbit.[1] In the left-hand panel of Fig. 1, the azimuths of the apocentre points do not cover the whole $[0, 2\pi]$ range, but rather oscillate within the interval $[-\phi_{max}, \phi_{max}]$. The orbit is said to be 'trapped' at a resonance, in this case the outer Lindblad resonance (see below), and the angle of the apocentres, the 'precession angle', is said to 'librate'. For comparison, the right-hand panel of Fig. 1 shows an orbit for which the precession angle covers the whole $[0, 2\pi]$ range. This orbit is said to 'circulate'. In the following, we give a quantitative description of these two types of orbits, using perturbation theory.

3 REDUCTION TO A PENDULUM

We will hereafter work within the epicyclic approximation (Binney & Tremaine 2008), in which radial oscillations are harmonic with angular frequency $\kappa(R)$, so the radial action $J_R = E_R/\kappa$, where $E_R = E - E_c$ is the energy of these oscillations (E_c being the energy of a circular orbit with the same angular momentum J_ϕ). Using the formulae reported in Dehnen (1999) and Monari et al. (2017a), we can then relate the coordinates of the trapped orbit to the angles θ_R and θ_ϕ of the unperturbed system. We can also rewrite the perturbing potential in the Galactic plane in terms of actions and angles as a Fourier series

$$\Phi_1(J_R, J_\phi, \theta_R, \theta_\phi) = \mathrm{Re}\left\{ \sum_{j=-1}^{1} c_{jm} \mathrm{e}^{\mathrm{i}[j\theta_R + m(\theta_\phi - \Omega_b t)]} \right\}, \tag{4}$$

with

$$c_{jm}(J_R, J_\phi) \equiv \left[\delta_{j0} + \delta_{|j|1}\frac{m}{2}\mathrm{sgn}(j)\gamma e\right]\Phi_a(R_g, 0) - \delta_{|j|1}\frac{R_g}{2}e\frac{\partial\Phi_a}{\partial R}(R_g, 0). \tag{5}$$

Here the guiding radius $R_g(J_\phi)$ is defined by $R_g^2\Omega(R_g) = J_\phi$, the eccentricity by $e(J_R, J_\phi) = \sqrt{2J_R/(\kappa R_g^2)}$ and $\gamma = 2\Omega(R_g)/\kappa(R_g)$.[2] In the epicyclic approximation, the radial and azimuthal frequencies of an orbit of actions (J_R, J_ϕ) are $\Omega_R = \kappa(R_g)$ and $\Omega_\phi = \Omega(R_g) + [\mathrm{d}\kappa(R_g)/\mathrm{d}J_\phi]J_R$, respectively.

At a resonance, the orbital frequencies Ω_R and Ω_ϕ satisfy

$$l\Omega_R + m(\Omega_\phi - \Omega_b) = 0. \tag{6}$$

The three main resonances are the corotation resonance ($l = 0$), and the outer ($l = 1$) and inner ($l = -1$) Lindblad resonances. To capture the behaviour of the slow- and fast-varying motions near the resonances, one makes a canonical transformation of coordinates defined by the following time-dependent generating function of type 2 (e.g. Weinberg 1994):

$$S(\theta_R, \theta_\phi, J_s, J_f, t) = \left[l\theta_R + m\left(\theta_\phi - \Omega_b t\right)\right] J_s + \theta_R J_f. \tag{7}$$

The new angles and actions $(\theta_f, \theta_s, J_f, J_s)$ are then related to the old ones by

$$\begin{aligned} \theta_s &= l\theta_R + m(\theta_\phi - \Omega_b t), & J_\phi &= mJ_s, \\ \theta_f &= \theta_R, & J_R &= lJ_s + J_f. \end{aligned} \tag{8}$$

By taking the time-derivative of θ_s in the unperturbed system, and by the definition of the resonance in equation (6), one finds that the evolution of the new 'slow' angle θ_s is indeed slow near a resonance. Given that along nearly circular orbits $\theta_\phi \simeq \phi$, from equation (8), we can understand why θ_s represents the azimuth of the apocentres and pericentres[3] of the orbit in the frame of reference that corotates with the bar: At $\theta_R = 0$ ($\theta_R = -\pi$), we are at the pericentre (apocentre) of the orbit and θ_s ($\theta_s + \pi$) is m times the star's azimuth $\theta_\phi - \Omega_b t$ in the frame of reference corotating with the orbit.

In the new canonical coordinates of equation (8), the motion in the perturbed system is described by the following Hamiltonian (also called the Jacobi integral):

$$H = H_0 + \mathrm{Re}\left\{ \sum_{j=-1}^{1} c_{jm} \mathrm{e}^{\mathrm{i}[(j-l)\theta_f + \theta_s]} \right\} - m\Omega_b J_s, \tag{9}$$

where H_0 is the Hamiltonian of the unperturbed axisymmetric system and the c_{jm} coefficients are the Fourier coefficients from equation (5), expressed as functions of the actions (J_f, J_s), thanks

[1] While in an axisymmetric potential the apocentres of the orbits in the Galactic plane are always at the same distance R from the Galactic Centre, this is not the case in a non-axisymmetric potential like the one used in this work. Therefore, the plotted points correspond to relative apocentres.

[2] In the potential from equation (1), $\kappa = \sqrt{2}\Omega$, so $\gamma = \sqrt{2}$.

[3] According to the convention of Dehnen (1999), in this work the angle $\theta_R = 0$ at the pericentre, and $\theta_R = \pi$ at the apocentre.

to the canonical transformation from equation (8). Since θ_f evolves much faster than θ_s, we average H along θ_f (the averaging principle, e.g. Arnold 1978; Weinberg 1994; Binney & Tremaine 2008), to obtain

$$\overline{H} = H_0(J_f, J_s) - m\Omega_b J_s + \mathrm{Re}\left\{c_{lm}(J_f, J_s)e^{i\theta_s}\right\}. \quad (10)$$

Since $\dot{J}_f = -\partial\overline{H}/\partial\theta_f = 0$, J_f is an integral of motion, and for each J_f, the motion of every orbit can be described purely in the (θ_s, J_s) plane.

For each value of J_f, let us then define $J_{s,res}$ as the value of J_s where

$$\Omega_s(J_f, J_{s,res}) = 0, \quad (11)$$

where $\Omega_s \equiv l\Omega_R + m(\Omega_\phi - \Omega_b)$. While we expand $H_0 - m\Omega_b J_s$ in a Taylor series of J_s around $J_{s,res}$ up to the second order, we estimate c_{lm} at $J_{s,res}$. Dropping the constant terms, we obtain the approximate Hamiltonian near the resonances (Chirikov 1979; Kaasalainen 1994):

$$\widehat{H} = \frac{1}{2}G\left(J_s - J_{s,res}\right)^2 - F\cos\left(\theta_s + g\right), \quad (12)$$

where

$$F \equiv -|c_{lm}\left(J_f, J_{s,res}\right)|, \quad G \equiv \frac{\partial\Omega_s}{\partial J_s}\left(J_f, J_{s,res}\right), \quad (13)$$

and $g \equiv \arg\left(c_{lm}(J_f, J_{s,res})\right)$. Equation (12) is the Hamiltonian of a pendulum, and the equations of motion are

$$\begin{aligned}\dot{\theta}_s &= G\left(J_s - J_{s,res}\right),\\ \dot{J}_s &= -F\sin\left(\theta_s + g\right).\end{aligned} \quad (14)$$

Combining them, we obtain the equation for the θ_s acceleration, namely

$$\ddot{\theta}_s = -\omega_0^2\sin\left(\theta_s + g\right), \quad (15)$$

where $\omega_0^2 \equiv FG$ (notice that in galaxies both F and G are negative).

The energy of the pendulum from equation (15) is

$$E_p = \frac{\dot{\theta}_s^{\,2}}{2} + V_p(\theta_s), \quad (16)$$

where

$$V_p(\theta_s) = -\omega_0^2\cos(\theta_s + g). \quad (17)$$

We can define the dimensionless quantity related to the energy

$$k = \sqrt{\frac{1}{2}\left(1 + \frac{E_p}{\omega_0^2}\right)}. \quad (18)$$

For $k < 1$, the orbit is trapped and librates around $\theta_s = -g$. In this regime, the solution of equation (14) is (e.g. Lawden 1989)

$$\theta_s + g = 2\arcsin\left(k\mathrm{sn}\left(\omega_0 t + C, k^2\right)\right), \quad (19)$$

$$J_s - J_{s,res} = J_a\mathrm{cn}\left(\omega_0 t + C, k^2\right), \quad (20)$$

where $J_a \equiv 2\sqrt{F/G}k$, and C is the phase of the orbit. The frequency of the oscillations of the librating pendulum is

$$\omega = \omega_0\frac{\pi}{2\mathrm{K}(k^2)}. \quad (21)$$

The Jacobi functions sn, cn and K are defined in Appendix A. Up to the second order, the expansion of equations (19)–(20) in $k \ll 1$ leads to a solution equivalent to that of a harmonic oscillator

$$\theta_s + g \approx 2k\sin\left(\omega_0 t + C\right), \quad (22)$$

$$J_s - J_{s,res} \approx J_a\cos\left(\omega_0 t + C\right), \quad (23)$$

with frequency $\omega \approx \omega_0$.

In the circulating case, $k > 1$, the solution of equation (14) for J_s is

$$J_s - J_{s,res} = J_a\mathrm{dn}\left(\omega_0 k t + C, 1/k^2\right), \quad (24)$$

where the Jacobi dn function is also defined in Appendix A. While in this case θ_s is a monotonic function of time, J_s is an oscillating function of time around $\langle J_s\rangle$. For $k \gg 1$

$$J_s \approx J_{s,res} + J_a, \quad (25)$$

which means that the angular momentum ($J_\phi = mJ_s$) is conserved very far from the resonance, i.e. we recover the axisymmetric case.

As an example, in Fig. 2, we follow the evolution of $\theta_s + \pi$ (since $g = \pi$ in the case of the bar) and J_s with $(l, m) = (1, 2)$ for the trapped orbit of Fig. 1. The blue lines in these plots correspond to the orbit integrated numerically. We see that the motion in θ_s and J_s is a composition of high-frequency, low-amplitude oscillations (that are ignored, when invoking the averaging principle), and slow-frequency, high-amplitude oscillations. The pendulum approximation (orange lines) provides a description of the latter.[4]

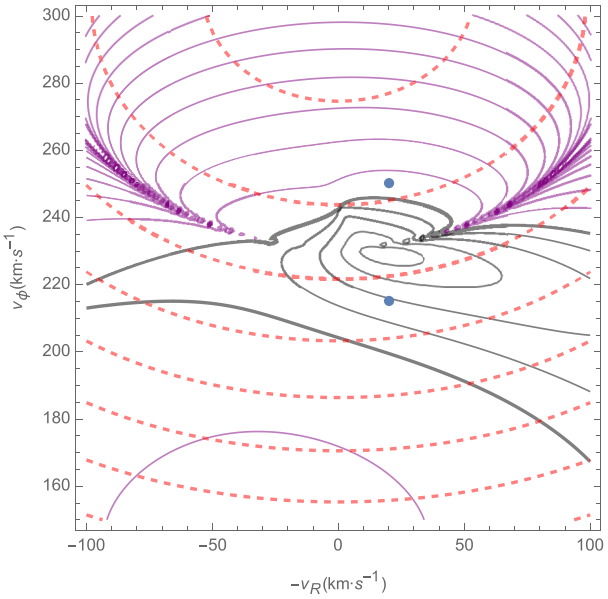

Figure 3. Contours of conserved quantities associated with the pendulum treatment at the outer Lindblad resonance in the $(-v_R, v_\phi)$ plane at $(R, \phi) = (8\ \mathrm{kpc}, -25^\circ)$ for the bar model presented in this work with $\Omega_b = 1.8\Omega_0$. The black contours correspond to constant values of k for $k \leq 1$. The thick black contour corresponds to $k = 1$. The purple contours correspond to constant values of k for $k > 1$. The red dashed contours correspond to constant values of J_f. The blue dots correspond to the initial conditions of the orbits shown in Fig. 1.

[4] A more accurate description of the orbit can be obtained by performing a limited development at higher order (Binney 2016).

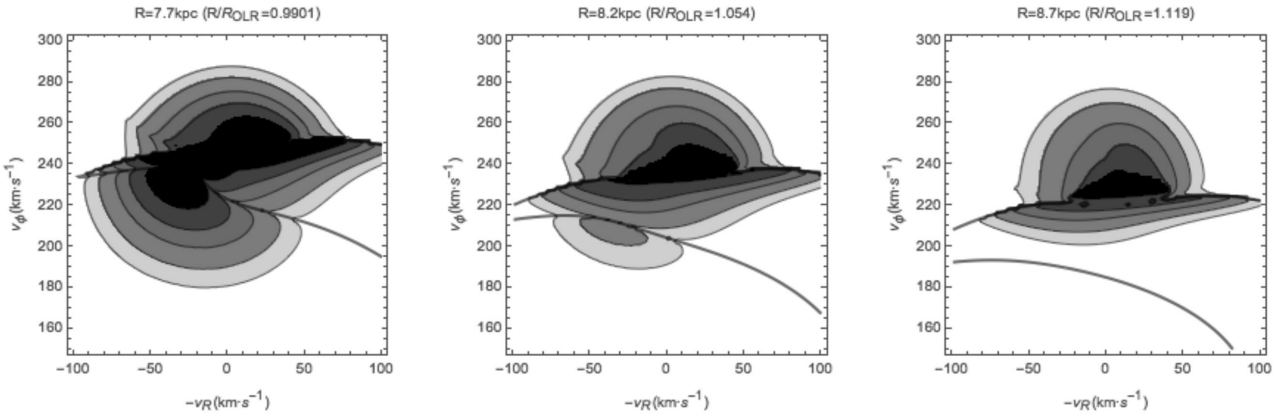

Figure 4. DF in the $(-v_R, v_\phi)$ plane at different Galactocentric radii R and $\phi = -25^\circ$, obtained using the treatment at the resonances and the bar model presented in this work. The bar's pattern speed is $\Omega_b = 1.8.\,\Omega_0$. The thick contours enclose orbits trapped at the outer Lindblad resonance. The DF contours enclose (from the outer to the inner) 95, 90, 80, 68 and 50 per cent of the stars.

4 ACTIONS AND ANGLES FOR THE PENDULUM

The action and the angle associated with the pendulum are (e.g. Brizard 2013), for the case $k < 1$,

$$J_p = \frac{4}{\pi}\frac{J_a}{k}\left[\mathrm{E}(k^2) - (1-k^2)\mathrm{K}(k^2)\right],$$
$$\theta_p = \frac{\pi}{2\mathrm{K}(k^2)}\mathrm{cn}^{-1}\left(\frac{J_s - J_{s,res}}{J_a}, k^2\right). \quad (26)$$

Using θ_p, we can rewrite $\theta_s + g$ as

$$\theta_s + g = 2\arcsin\left(k\mathrm{sn}\left(\frac{2}{\pi}\mathrm{K}(k^2)\theta_p, k^2\right)\right), \quad (27)$$

and

$$J_s - J_{s,res} = J_a\mathrm{cn}\left(\frac{2}{\pi}\mathrm{K}(k^2)\theta_p, k^2\right). \quad (28)$$

For the case $k > 1$, one has

$$J_p = \frac{2}{\pi}J_a\mathrm{E}(1/k^2), \theta_p = \frac{\pi}{\mathrm{K}(1/k^2)}\mathrm{dn}^{-1}\left(\frac{J_s - J_{s,res}}{J_a}, 1/k^2\right). \quad (29)$$

We can rewrite

$$J_s - J_{s,res} = J_a\mathrm{dn}\left(\frac{\mathrm{K}(1/k^2)}{\pi}\theta_p, 1/k^2\right). \quad (30)$$

In Fig. 3, we show k and J_f contours in the velocity space[5] $(-v_R, v_\phi)$, for $(R, \phi) = (8\ \mathrm{kpc}, -25^\circ)$ with the same potential as used to integrate the orbits in Fig. 1. The black contours are for $k < 1$ (trapped orbits) and the green contours for $k > 1$ (circulating orbits). The red-dashed contours correspond to contours of constant J_f. The quantities k (or J_p) and J_f characterize an orbit.[6] The blue points correspond to the initial conditions of the two orbits in Fig. 1, which both start from $(R, \phi) = (R_0, -25^\circ)$. The minimum $k = 0$ is found at $(-v_R, v_\phi) \approx (25\,230)\ \mathrm{km\,s^{-1}}$ and corresponds to the most trapped orbit at the outer Lindblad resonance for such (R, ϕ).

[5] The minus in front of v_R is chosen to allow a better comparison with the data of kinematics of stars in the Galaxy, usually plotted in the (U, V) space, with U positive towards the Galactic Centre.

[6] The quantity $J_{s,res}$ is fixed by J_f, from the condition $\Omega_s(J_f, J_{s,res}) = 0$.

5 AVERAGING DISTRIBUTION FUNCTIONS OVER PENDULUM ANGLES

Following the prescription of Binney (2016), we assume that the DF for orbits trapped by the resonances ($k < 1$) at a certain point (J_f, J_s, θ_s) is given by the average of the unperturbed DF f_0 along θ_p, i.e.

$$f_{tr}(J_f, J_s, \theta_s) = \frac{1}{2\pi}\int_0^{2\pi} f_0(J_f, J_{s,res} + \Delta J_s(\theta_p))\mathrm{d}\theta_p, \quad (31)$$

where from equation (30)

$$\Delta J_s \equiv J_a\mathrm{cn}\left(\frac{2}{\pi}\mathrm{K}(k^2)\theta_p, k^2\right), \quad (32)$$

and k is a function of (J_f, J_s), and θ_s, derived from R, ϕ, v_R, v_ϕ, and the potential. The physical meaning of equation (31) is that f_{tr} corresponds to the unperturbed DF f_0 phase-mixed along the pendulum angle, assuming that enough time elapsed since the growth of the perturbation.

The value of the integral in equation (31) depends on the particular form of f_0. Therefore, in general, its solution can be computed numerically as

$$f_{tr}(J_f, J_s, \theta_s) = \frac{1}{N}\sum_i f_0(J_f, J_{s,res} + \Delta J_s(\theta_p^i)), \quad (33)$$

where θ_p^i sample the orbit between 0 and 2π, and N is the number of sampling points.

For $k \ll 1$, we can even give an analytic form for the DF. To solve this integral, we expand $\ln(f_0)$ around $J_{s,res}$ (in typical galaxies f_0 is almost exponential in J_s) as

$$\ln\left(f_0(J_f, J_{s,res} + \Delta J_s)\right) \approx \ln\left(f_0(J_f, J_{s,res})\right) - \frac{\Delta J_s}{J_h}, \quad (34)$$

where

$$J_h \equiv -1\Big/\left(\frac{1}{f_0}\frac{\partial f_0}{\partial J_s}\right)_{J_{s,res}}. \quad (35)$$

Then

$$f_0(J_f, J_{s,res} + \Delta J_s) \approx f_0(J_f, J_{s,res})\mathrm{e}^{-\Delta J_s/J_h}. \quad (36)$$

This approximation is excellent to express f_0, but, unfortunately, it is not enough to solve the integral from equation (31). To do that,

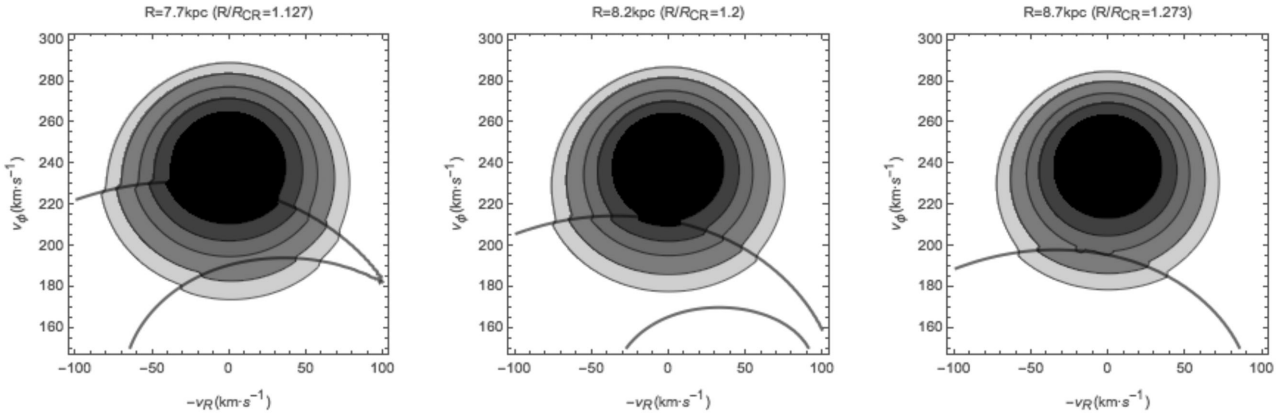

Figure 5. As in Fig. 4, but for a bar's pattern speed $\Omega_b = 1.2\,\Omega_0$. The thick contours enclose orbits trapped to the corotation.

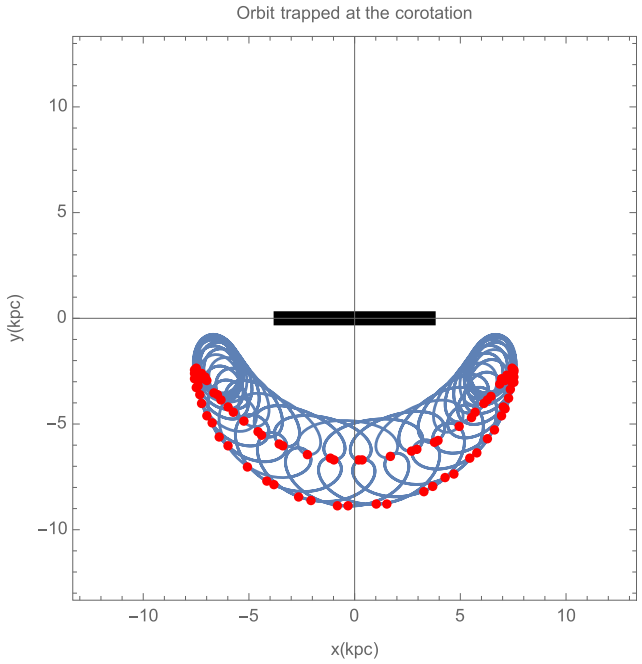

Figure 6. An orbit trapped to the corotation, integrated in the potential presented in this work with a bar's pattern speed $\Omega_b = 1.2\Omega_0$. The orbit is shown in the reference frame corotating with the bar. The initial conditions of this orbit are $(R, \phi) = (8.2\text{ kpc}, -25^\circ)$ and $(-v_R, v_\phi) = (-10, 210)\text{ km s}^{-1}$. The red dots correspond to the position of the apocentres and the black thick line to the long axis of the bar. The bar rotates counterclockwise.

one more approximation is necessary. Expanding equation (32) to first order in k, ΔJ_s can be expressed as

$$\Delta J_s \approx J_a \cos\theta_p, \tag{37}$$

In this way, *de facto*, we fall back on the harmonic oscillator solution equations (22)–(23). With these approximations, the solution of the integral from equation (31) is

$$f_{tr}(J_f, J_s, \theta_s) = f_0(J_f, J_{s,res})\mathrm{I}_0(J_a/J_h), \tag{38}$$

where $\mathrm{I}_0(x)$ is the incomplete Bessel function of the first kind.

For the zone of circulation ($k > 1$), we instead use for the DF the prescription

$$f_{circ}(J_f, J_s, \theta_s) = f_0(J_f, \overline{J_s}), \tag{39}$$

where

$$\overline{J_s} = \frac{1}{2\pi}\int_0^{2\pi} J_s(\theta_p)\mathrm{d}\theta_p = J_{s,res} + \frac{\pi}{2}\frac{J_a}{\mathrm{K}(1/k^2)}. \tag{40}$$

This prescription is motivated by the fact that, outside of the trapping region, the perturbing potential simply deforms the orbital tori of the underlying axisymmetric system rather than abruptly building completely new tori as it does within the trapping region. Consequently, if the perturbation emerges slowly enough, the phase-space density will be adiabatically constant on each torus as it is deformed at its original value, $f_0(\boldsymbol{J})$, where $\boldsymbol{J} = (J_f, \overline{J_s})$ is to be understood to be the invariant actions of the perturbed torus rather than momenta of the original system of angle–action variables. Notice that, for large k (far from the resonance), $\overline{J_s} \to J_s$ rather fast, and we are back to the axisymmetric case (conservation of the angular momentum $J_\phi = mJ_s$).

6 RESULTS

We now present a few results of astrophysical interest for the response at the resonances of an unperturbed DF f_0 to the bar perturbation presented in the previous sections.

As an unperturbed DF f_0 we choose (Binney & McMillan 2011)

$$f_0(J_R, J_\phi) = \frac{\gamma(R_g)\Sigma_0 \mathrm{e}^{-R_g/h_R}}{2\pi\sigma_R^2(R_g)} \mathrm{e}^{-\frac{J_R\kappa(R_g)}{\sigma_R^2(R_g)}}, \tag{41}$$

where

$$\sigma_R(R) = \sigma_R(R_0)\mathrm{e}^{-\frac{R-R_0}{5h_R}}, \tag{42}$$

with γ defined as in equation (5), $\sigma_R(R_0) = 30\text{ km s}^{-1}$ and $h_R = 2$ kpc, a reasonable description of the kinematics of the solar neighbourhood.

We first consider, in Fig. 4, the density of stars in local velocity space obtained from a model with a 'fast' rotating bar, as in the classical picture (Dehnen 2000; Antoja et al. 2014; Monari et al. 2017b). For such a bar, the solar neighbourhood is in the vicinity of the outer Lindblad resonance of the bar. The angle of the bar with respect to the solar position is taken to be $\phi = -25^\circ$. The bar that we present here has $\Omega_b = 1.8\,\Omega_0$. We see that, in line with previous studies, the analysis in this work also predicts the formation of a low-velocity overdensity similar to the Hercules moving group (e.g. Dehnen 1998; Famaey et al. 2005) at positive v_R, whose velocity position and relative amplitude vary as a function of radius. The group is not formed

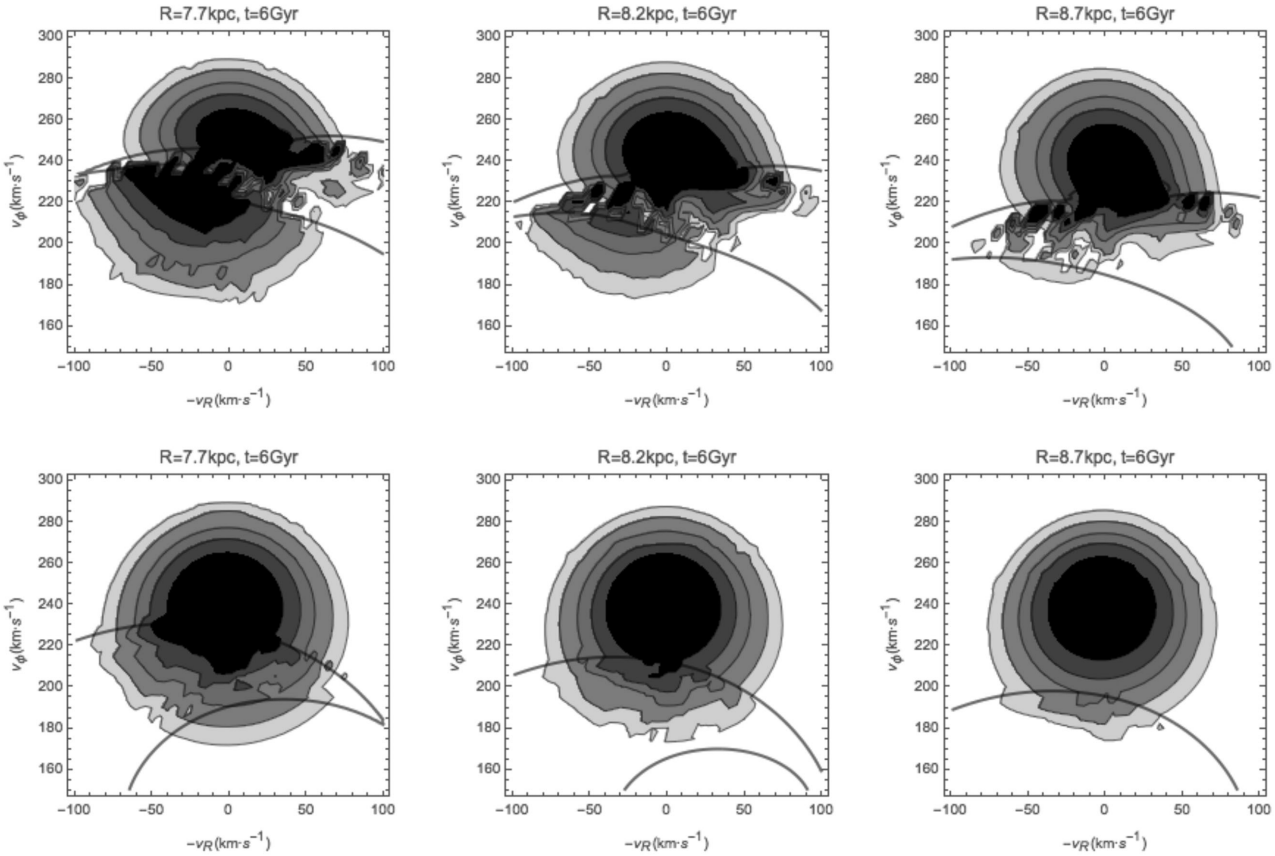

Figure 7. Local velocity distribution obtained from numerically integrating orbits for 6 Gyr after an adiabatic growth of the bar, starting from the same initial f_0 DF as for Figs 4 and 5. The resolution of the grid used to obtain this figure is 5 km s^{-1}. Compare the top row ($\Omega_b = 1.8\Omega_0$) with Fig. 4, and the bottom row ($\Omega_b = 1.2\Omega_0$) with Fig. 5.

by orbits trapped by the outer Lindblad resonance but from circulating orbits with guiding radii inside the R_{OLR}. The orbits trapped to a resonance rather seem to be associated with the feature of local velocity space sometimes called the 'horn' (e.g. Monari 2014). This is also in line with previous studies, but never before had the DF in the trapped region been quantified for a fully phase-mixed population. Interestingly, we clearly see that in this case the Hercules moving group shifts both in v_ϕ (lower v_ϕ at larger radii) and in $-v_R$ (larger $-v_R$ at larger radii).

Recently, Sormani, Binney & Magorrian (2015) and Li et al. (2016) have argued that the pattern speed of the bar is $\Omega_b = 1.2\Omega_0$, significantly lower than in the classical picture. In this case, the solar neighbourhood would lie just outside corotation, so in Fig. 5, we also plot the velocity distribution at three such locations. In the central and right-hand panels of Fig. 5, when the zone of trapping is at low azimuthal velocities, a deformation in the velocity distribution at negative $-v_R$ that could resemble Hercules forms *within* the trapping zone rather than outside it. When there is a region of enhanced density below the trapping zone, (left-hand panel of Fig. 5), it occurs at $-v_R > 0$, as predicted by the *Eulerian* linear theory, and as such conflicts with the observations. Hence, the pendulum formalism is mandatory if one seeks to explain the Hercules group as a consequence of the corotation resonance, as Pérez-Villegas et al. (2017) did with made-to-measure *N*-body models. Note that the orbits associated with the overdensity at $(-v_R, v_\phi) \approx (-10, 210)$ km s^{-1} in the central panel of Fig. 5 are of the same kind as those described by Pérez-Villegas et al. (2017), i.e. trapped around the bar's Lagrangian points (see Fig. 6). Finally, we provide the reader with a comparison plot in Fig. 7, in which we display the local velocity distribution obtained from orbits integrated for 6 Gyr in the same potential, after the bar is slowly grown for 3 Gyr with the growth law from Dehnen (2000), and for the same initial f_0 as in our analytic model (with the backward integration method of Vauterin & Dejonghe 1997; Dehnen 2000).

7 CONCLUSION

In this paper, we presented for the first time a way to treat an action-based DF in the region of action space where orbits are resonantly trapped by a bar, where the *Eulerian* treatment of Monari et al. (2016) diverges. The idea is rather to follow the deformation of the tori outside the trapping region while averaging the DF over the relevant angles in the trapping region. We showed that in the trapping region the relevant action–angle variables are those of a pendulum, and averaging over those angles allows us for a smooth connection with the deformed tori in the circulation zone. With such DFs, we can reproduce an overdensity in velocity space resembling the Hercules moving group both outside the outer Lindblad resonance and outside the corotation of a bar. The linearized *Eulerian* treatment of Monari et al. (2017a) is unable to handle the latter possibility. The disturbances in velocity space that are caused by the inner Lindblad and corotation resonances move in different ways through velocity

space as one changes location within the disc (Figs 4 and 5). Consequently, it will be straightforward to determine which resonance is responsible for the Hercules group, once we can reliably map velocity space in many locations.

This formalism opens the way to fitting quantitatively the effects of the bar in an action-based modelling of the Milky Way. Nevertheless, there remain multiple tests to be done, which are beyond the scope of the present contribution presenting the relevant formalism. In particular, the prediction of a fully phase-mixed DF in the trapping region should be compared to the outcome of various simulations, to check over which time-scales phase-mixing is efficient enough to reproduce our results. Moreover, the process of trapping and the associated filling of the region of resonant trapping in action space is not necessarily going to be based purely on the phase-mixing of the original axisymmetric DF, especially if the growth of the bar is rapid. But even in this case, the advantage of this present paper has been to present the relevant pendulum action variables on which to base a parametric DF to fit both simulations and real data in the trapping zone.

As a matter of fact, only the upcoming *Gaia* data will allow us to check whether our phase-mixing of the original DF is actually a good representation of the Galactic disc at different radii. If not, knowing that our DF must depend only on the new set of action variables within the trapping region, we will be able to leave its functional form free, and fit it to the data. This approach is very fast and does not require to perform numerous expensive simulations. As a consequence, one will be able to explore very efficiently the parameter space of the perturbations.

Further improvements of the present formalism will need taking into account the vertical z direction, the time dependence in the amplitude of perturbations, as well as collective effects (e.g. Weinberg 1989; Fouvry et al. 2015). It will also be mandatory to move away from the epicyclic approximation (McGill & Binney 1990; Sanders & Binney 2015). Once this will be done, in the absence of strong resonance overlaps, a complete dynamical model of the present-day Milky Way disc could then, in principle, finally be built by applying, on top of the trapped DF near the main resonances of each perturber, our previous *Eulerian* treatment of perturbations (Monari et al. 2016) for the other perturbers, even including vertical perturbations and 'bending' modes of the disc (Widrow et al. 2014; Xu et al. 2015; Laporte et al. 2016).

ACKNOWLEDGEMENTS

J-BF acknowledges support from Programme HST-HF2-51374, which was provided by NASA through a grant from the Space Telescope Science Institute, which is operated by the Association of Universities for Research in Astronomy, Incorporated, under NASA contract NAS5-26555. This work was supported by the European Research Council under the European Union's Seventh Framework Programme (FP7/2007-2013)/ERC grant agreement no. 321067.

REFERENCES

Antoja T. et al., 2014, A&A, 563, A60
Arnold V. I., 1978, Mathematical Methods of Classical Mechanics. Springer-Verlag, New York
Aumer M., Binney J., 2017, MNRAS, 470, 2113
Aumer M., Binney J., Schönrich R., 2016, MNRAS, 462, 1697
Binney J., 2016, MNRAS, 462, 2792
Binney J., McMillan P., 2011, MNRAS, 413, 1889
Binney J., Piffl T., 2015, MNRAS, 454, 3653
Binney J., Tremaine S., 2008, Galactic Dynamics, 2nd edn. Princeton Univ. Press, Princeton, NJ
Binney J., Gerhard O. E., Stark A. A., Bally J., Uchida K. I., 1991, MNRAS, 252, 210
Binney J., Gerhard O., Spergel D., 1997, MNRAS, 288, 365
Bovy J., Bird J. C., García Pérez A. E., Majewski S. R., Nidever D. L., Zasowski G., 2015, ApJ, 800, 83
Brizard A. J., 2013, Commun. Nonlinear Sci. Numer. Simul., 18, 511
Chirikov B. V., 1979, Phys. Rep., 52, 263
Cole D. R., Binney J., 2017, MNRAS, 465, 798
de Vaucouleurs G., 1964, in Kerr F. J., ed., Proc. IAU Symp. 20, The Galaxy and the Magellanic Clouds. Australian Academy of Sciences, Canberra, p. 195
Dehnen W., 1998, AJ, 115, 2384
Dehnen W., 1999, AJ, 118, 1190
Dehnen W., 2000, AJ, 119, 800
Famaey B., Jorissen A., Luri X., Mayor M., Udry S., Dejonghe H., Turon C., 2005, A&A, 430, 165
Fouvry J. B., Pichon C., Magorrian J., Chavanis P. H., 2015, A&A, 584, A129
Fouvry J.-B., Binney J., Pichon C., 2015, ApJ, 806, 117
Fouvry J.-B., Pichon C., Prunet S., 2015, MNRAS, 449, 1967
Gaia Collaboration et al., 2016, A&A, 595, A1
Grand R. J. J., Bovy J., Kawata D., Hunt J. A. S., Famaey B., Siebert A., Monari G., Cropper M., 2015, MNRAS, 453, 1867
Kaasalainen M., 1994, MNRAS, 268, 1041
Laporte C. F. P., Gómez F. A., Besla G., Johnston K. V., Garavito-Camargo N., 2016, MNRAS, preprint (arXiv:1608.04743)
Lawden D., 1989, Elliptic Functions and Applications: Applied Mathematical Sciences. Springer-Verlag, New York
Li Z., Gerhard O., Shen J., Portail M., Wegg C., 2016, ApJ, 824, 13
McGill C., Binney J., 1990, MNRAS, 244, 634
McMillan P. J., 2013, MNRAS, 430, 3276
Monari G., 2014, PhD thesis, Rijksuniversiteit Groningen
Monari G., Famaey B., Siebert A., 2015, MNRAS, 452, 747
Monari G., Famaey B., Siebert A., 2016, MNRAS, 457, 2569
Monari G., Famaey B., Siebert A., Grand R. J. J., Kawata D., Boily C., 2016, MNRAS, 461, 3835
Monari G., Famaey B., Siebert A., Duchateau A., Lorscheider T., Bienaymé O., 2017a, MNRAS, 465, 1443
Monari G., Kawata D., Hunt J. A. S., Famaey B., 2017b, MNRAS, 466, L113
Pérez-Villegas A., Portail M., Wegg C., Gerhard O., 2017, ApJ, 840, L2
Sanders J. L., Binney J., 2015, MNRAS, 447, 2479
Sellwood J. A., Carlberg R. G., 2014, ApJ, 785, 137
Sormani M. C., Binney J., Magorrian J., 2015, MNRAS, 454, 1818
Trick W. H., Bovy J., D'Onghia E., Rix H.-W., 2017, ApJ, 839, 61
Vauterin P., Dejonghe H., 1997, MNRAS, 286, 812
Wegg C., Gerhard O., Portail M., 2015, MNRAS, 450, 4050
Weinberg M. D., 1989, MNRAS, 239, 549
Weinberg M. D., 1994, ApJ, 420, 597
Widrow L. M., Barber J., Chequers M. H., Cheng E., 2014, MNRAS, 440, 1971
Williams M. E. K. et al., 2013, MNRAS, 436, 101
Xu Y., Newberg H. J., Carlin J. L., Liu C., Deng L., Li J., Schönrich R., Yanny B., 2015, ApJ, 801, 105

APPENDIX A: JACOBI SPECIAL FUNCTIONS

The Jacobi sn, cn and dn functions can be evaluated as the sum of a power series, and are defined as

$$\mathrm{sn}(u, m) \equiv \sin(\varphi), \quad \mathrm{cn}(u, m) \equiv \cos(\varphi), \tag{A1}$$

with

$$u = \int_0^{\varphi} \frac{\mathrm{d}\theta}{\sqrt{1 - m \sin^2 \theta}}. \tag{A2}$$

The dn function is defined as

$$\mathrm{dn}(u, m)^2 \equiv 1 - m\mathrm{sn}^2(u, m). \tag{A3}$$

The elliptic functions E and K are defined as

$$\mathrm{E}(m) = \int_0^{\pi/2} \mathrm{d}\theta \sqrt{1 - m \sin^2 \theta}, \tag{A4}$$

$$\mathrm{K}(m) = \int_0^{\pi/2} \frac{\mathrm{d}\theta}{\sqrt{1 - m \sin^2 \theta}}. \tag{A5}$$

This paper has been typeset from a TEX/LATEX file prepared by the author.